Metallophysics and Advanced Technologies
Металофіз. новітні технол.
Metallofiz. Noveishie Tekhnol.
2025, vol. 47, No. 3, pp. 257–270
https://doi.org/10.15407/mfint.47.03.0257
Reprints available directly from the publisher

PACS numbers: 61.66.Dk, 61.72.Ff, 62.20.Qp, 81.20.Ev, 81.40.Cd, 81.40.Lm, 81.70.Bt

Sintered Al–Si–Ni Alloy: Structure and Properties. II. Sintering and Forging

V. V. Kaverinsky, G. A. Bagliuk, S. F. Kyrylyuk, D. G. Verbylo, Z. P. Sukhenko, I. M. Kirian*, M. A. Skoryk*, and O. D. Rud*

I. M. Frantsevich Institute for Problems in Materials Science, N.A.S. of Ukraine, 3 Omeljan Pritsak Str., UA-03142 Kyiv, Ukraine
**G. V. Kurdyumov Institute for Metal Physics, N.A.S. of Ukraine, 36 Academician Vernadsky Blvd., UA-03142 Kyiv, Ukraine*

The presented study focuses on the development of a high-silicon Al–Si–Ni alloy with a coefficient of thermal expansion (CTE) comparable to that of steels, using powder metallurgy techniques. Experimental investigations are conducted to evaluate the effects of different sintering regimes—both liquid phase and solid one—on materials fabricated from elemental powder mixtures and ball-milled pre-alloyed powders. The results indicate that the optimal properties are achieved using a solid-phase sintering process followed by hot side setting and hot forging. This method results in a non-porous material with homogeneously distributed, fine spherical silicon inclusions, ranging from 1 to 7 μm in size. Liquid-phase sintering is revealed impractical due to exudation, which leads to chemical-composition misrepresentation and the formation of course, cast-like structures with reduced mechanical properties. The use of pre-alloyed powders is determined to be preferable over elemental powder mixtures, as the latter results in porous materials with coarse intermetallic aggregates. The final alloy exhibits high mechanical properties, including yield strength of ≅ 221 MPa, ultimate tensile strength of ≅ 261 MPa, and hardness of ≅ 96 *HB*, alongside a CTE suitable for industrial applications.

Key words: Al–Si–Ni alloy, powder metallurgy, thermal expansion coeffi-

Corresponding author: Oleksandr Dmytrovych Rud
E-mail: rud@imp.kiev.ua

Citation: V. V. Kaverinsky, G. A. Bagliuk, S. F. Kyrylyuk, D. G. Verbylo, Z. P. Sukhenko, I. M. Kirian, M. A. Skoryk, and O. D. Rud, Sintered Al–Si–Ni Alloy: Structure and Properties. II. Sintering and Forging, *Metallofiz. Noveishie Tekhnol.*, **47**, No. 3: 257–270 (2025). DOI: 10.15407/mfint.47.03.0257

cient, sintering techniques, mechanical properties.

У даному дослідженні зосереджено увагу на розробці висококремнійового стопу Al–Si–Ni з коефіцієнтом теплового розширення (КТР), близьким до КТР криці, з використанням технологій порошкової металурґії. Проведено експериментальні дослідження для оцінки впливу різних режимів спікання як у рідкій, так і в твердій фазах на матеріяли, виготовлені з порошкових сумішей елементарних компонентів і подрібнених порошків попередньо виготовленого стопу. Результати показали, що оптимальні властивості досягнуто за допомогою процесу спікання у твердій фазі з подальшим гарячим пресуванням і штампуванням. Цей метод дав змогу одержати матеріял з однорідно розподіленими дрібними сферичними включеннями силіцію розміром від 1 до 7 мкм. Спікання в рідкій фазі виявилося недоцільним через явище випотівання, яке призводить до спотворення хемічного складу та формування грубих структур литого типу з пониженими механічними властивостями. Використання порошків стопу було визнано ліпшим, аніж сумішей елементарних компонентів, оскільки останні приводять до утворення пористих матеріялів з грубими інтерметалевими аґреґатами. Одержаний стоп демонструє високі механічні властивості, включаючи межу плинности у ≅ 221 МПа, межу міцности за розтягу у ≅ 261 МПа і твердість у ≅ 96 *HB*, а також КТР, що відповідає вимогам промислових виробників.

Ключові слова: стоп Al–Si–Ni, порошкова металурґія, коефіцієнт теплового розширення, методи спікання, механічні властивості.

(Received 20 August, 2024; in final version, 22 October, 2024)

1. INTRODUCTION

The advancement of industry heavily relies on the introduction of new materials with distinct physical, mechanical, and functional properties [1–3]. A significant focus is directed towards the development of innovative technologies for producing modern metallic and metal-composite materials, to enhance their physical and chemical properties. The necessity for novel materials arises from the imperative to improve product characteristics, expand the operational temperature range, and protect equipment from destabilising factors during use. Of particular interest for the manufacturing of precision orientation and navigation instruments in space applications are aluminium-based composite materials that exhibit a reduced coefficient of thermal expansion (CTE) coupled with high resistance to microdeformation.

A promising approach to developing lightweight, corrosion-resistant materials with a low CTE is through the utilisation of hypereutectic alloys within the Al–Si system. This approach is largely favoured due to the almost proportional reduction in CTE with increasing silicon concentration, given that the CTE of silicon is approximate-

ly six times lower than that of aluminium [4]. However, conventional casting methods used for alloys with silicon content exceeding 15% often result in the formation of coarse primary crystals, which significantly degrade the mechanical and technological properties of the material. Furthermore, increasing the silicon content beyond 20–22% exacerbates zonal segregation [4, 5]. Despite the availability of various modification techniques aimed at refining the morphology of the coarse silicon component, traditional methods have yet to produce high-silicon alloys that fully meet the desired quality and property standards.

Powder metallurgy presents a viable solution to the aforementioned challenges in producing the required materials. However, the practical implementation of this approach introduces numerous challenges that necessitate comprehensive research in metal physics and materials science. The preceding phase of this study focused on the development of pre-alloyed powder, which serves as the raw material for subsequent product manufacturing. Nonetheless, additional questions and challenges arise concerning the technology used for producing the final material. Key considerations include determining the optimal sintering temperature and duration, assessing the relative merits of solid-state versus liquid-phase sintering, deciding between using a mere mixture of components or producing a master alloy, addressing potential porosity, and ensuring that the mechanical properties of the alloy are satisfactory, along with strategies for their enhancement. This segment of the study aims to address these questions and develop a suitable technology for producing such materials.

The literature lacks consensus on the suitability of liquid-phase versus solid-state sintering regimes for aluminium-based powder materials. Studies have investigated the sintering of Al–Si, Al–Cu, Al–Si–Cu, and Al–Zn alloys in the presence of a liquid phase, as reported in works [6–10]. These studies highlight the positive effects of liquid-phase sintering, such as the reduction of material porosity through pore filling by the melt. However, it is important to note that these studies focused on alloys with different chemical compositions, characterised by lower silicon content (no more than 12–14%), the absence or significantly lower content of nickel, and the presence of other alloying elements such as copper, zinc, or magnesium. As such, the recommendations derived from these studies cannot be directly applied to the material under consideration without verification and modification.

Hot deformation processing is one potential method for mitigating porosity in powder materials. However, Al–Si materials are known for their brittleness, which may necessitate a specialised technique for hot deformation. Despite these challenges, it remains feasible, and our prior research on the deformation-heat treatment of Al–Si alloys—albeit with lower silicon content in cast alloys—yielded some promising results in terms of structural and property improvements [11]. In

this study, such a method will be applied to materials produced via powder metallurgy, with significantly higher silicon content.

The primary objective of this segment of the study is to develop approaches for the manufacture of Al–Si–Ni sintered alloys and to establish a robust technique that produces high-quality materials suitable for use in precision device constructions.

2. MATERIALS AND METHODS

The present study investigates two principal approaches: the fabrication of materials using a mixture of elemental component powders, and the utilisation of powder produced by grinding melt-spun ribbons of the master alloy. For the first method, aluminium (Al) powder with an average particle size of approximately 147 μm, silicon (Si) powder of around 11 μm, and nickel (Ni) powder of about 76 μm were employed. In the second approach, the powder was generated by mechanically grinding the melt-spun ribbons of the Al–Si–Ni alloy using a Fritsch Pulverisette P-6 planetary ball mill equipped with a stainless steel bowl. The detailed procedure for obtaining the powder was delineated in the previous part of this study [12]. The resulting powder particles had an average size of approximately 180 μm. The chemical compositions of the powders utilised in this study are presented in Table 1.

The powders were compacted under a pressure range of 500–600 MPa into shells fabricated from low-carbon steel. The inclusion of these shells facilitates subsequent hot deformation treatment. Their presence is presumed to optimize the deformation process, making it more akin to the mode of all-around compression, which is critical for materials with inherent brittleness. The briquettes encased in steel shells had an outer diameter of 32 mm, an inner diameter of 28 mm, a height of 37 mm (including the bottom and cover), and a cover thickness of 1.5 mm. The bottom section was welded to the sidewall of the shell before pressing. After pressing and sintering, a cover was pressed onto the specimens and subsequently welded. A series of samples was prepared under the conditions outlined in Table 2.

A specialised die was constructed to facilitate the hot deformation processing. Images of its components are provided in Fig. 1. The temperature for the hot deformation ranged between 520 and 540°C.

TABLE 1. Chemical composition of the starting materials used for specimen fabrication, % wt.

Material type	Al	Si	Ni
Grinded melt-spun ribbon obtained from the Al–Si–Ni alloy	Base	31.32	6.51
Mixture of elemental powders		32.91	5.91

TABLE 2. The sample conditions preparation.

Sample number	Preparation conditions
1	Fabricated from the powder mixture, solid-phase sintering at 350°C (≅ 30 minutes) + 530°C (≅ 2 hours) and forging at 530–540°C
2	Fabricated from pre-alloyed powder, solid-phase sintering at 350°C (≅ 30 minutes) + 530°C (≅ 2 hours) and forging at 520°C
3	Fabricated from pre-alloyed powder, liquid-phase sintering at 560°C (40–45 minutes) and forging at 530–540°C
4	Fabricated from pre-alloyed powder, liquid-phase sintering at 560°C (40–45 minutes) and forging at 520°C, with prior side pressing at 510–520°C
5	Fabricated from the powder mixture, liquid-phase sintering at 560–580°C (≅ 40 minutes) without forging

Dilatometric measurements were conducted using a dilatometer equipped with an inductive transducer, with a relative measurement error of ±0.5%. Mechanical testing was performed on cylindrical samples with a gauge length $l_0 = 20$ mm and diameter $d_e = 3$ mm at a strain rate $e = 2 \cdot 10^{-3}$ s^{-1}. The phase composition of the alloys was analysed using a ДРОН-4 diffractometer with radiation MoK_α. The x-ray diffraction (XRD) patterns were processed using the Rietveld refinement method with MAUD software [13].

Electron microscopy and x-ray microanalysis of the present phases and structural entities were performed using a TESCAN MIRA 3 microscope. The microstructure of the samples was examined using an

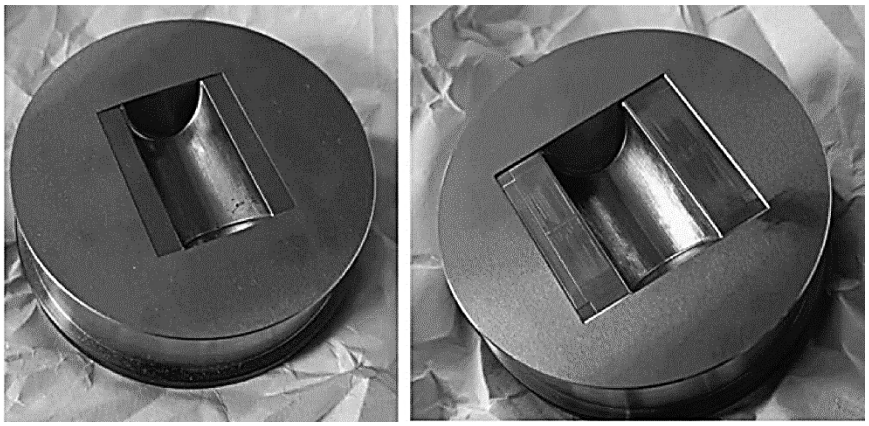

Fig. 1. Images of the die components used for the hot deformation treatment of samples.

'Optima Biofinder Bino' optical microscope, equipped with a 'SIGETA' digital ocular camera (model MC200).

3. RESEARCH RESULTS AND DISCUSSION

X-ray diffraction (XRD) patterns of the synthesised samples are illustrated in Fig. 2. The optimal Rietveld refinement for all sintered samples revealed three primary phases: an Al solid solution, Si, and the intermetallic compound $NiAl_3$. Notably, sample No. 1, fabricated *via* solid-phase sintering from a mixture of elemental powders, also exhibited a minor phase of Ni (≅ 2% wt.) (Fig. 2, *a*). However, according to the Rietveld refinement analysis, the Ni phase was not detected in the other samples.

The results of the quantitative phase analysis are detailed in Table 3. Sample No. 1, synthesised from a mixture of elemental powders by solid-phase sintering, exhibited the lowest amount of $NiAl_3$, potentially due to incomplete intermetallic formation. Conversely, samples No. 2 and No. 5 demonstrated the highest $NiAl_3$ content, approximating the equilibrium phase amount for the studied composition.

The sintering method and initial materials exert a considerable influence on the crystallite sizes of the observed phases. The largest crystallite sizes for Al were found in samples No. 1 and No. 2, obtained

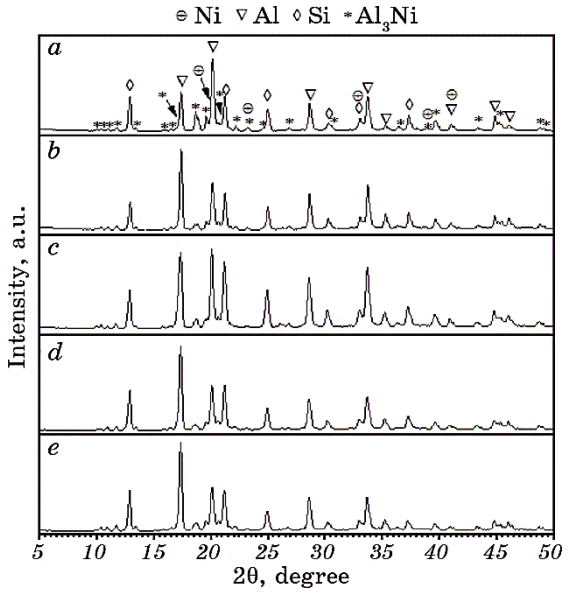

Fig. 2. Representative XRD patterns of sintered materials derived from powder mixtures (*a*, *e* for samples Nos. 1 and 5) and pre-alloyed powder (*b*–*d* for samples Nos. 2–4).

TABLE 3. Crystallographic parameters derived from Rietveld fitting of the XRD patterns of sintered samples.

Sample No.	Phase	Lattice parameters, Å			Crystallite size, Å	Abundance, % wt.	R_{wp}, %
		a	*b*	*c*			
1	Al	4.052	–	–	770	53	11.04
	Si	5.433	–	–	860	34	
	Al_3Ni	6.593	7.365	4.811	670	11	
	Ni	3.526	–	–	780	2	
2	Al	4.054	–	–	1070	58	12.5
	Si	5.433	–	–	1310	24	
	Al_3Ni	6.617	7.378	4.816	630	18	
3	Al	4.061	–	–	500	57	11.29
	Si	5.442	–	–	670	29	
	Al_3Ni	6.624	7.398	4.825	360	14	
4	Al	4.058	–	–	660	58	10.03
	Si	5.439	–	–	730	28	
	Al_3Ni	6.603	7.366	4.813	490	14	
5	Al	4.059	–	–	650	57	10.14
	Si	5.444	–	–	1025	26	
	Al_3Ni	6.623	7.389	4.831	600	17	

after solid-phase sintering from elemental powder (≅ 770 Å) and master alloy powder (≅ 1070 Å), respectively. Although the differences in crystallite sizes between samples subjected to different types of liquid-phase sintering were less pronounced, they were still observable. The crystallite sizes of Si in samples No. 1, No. 3, and No. 4 were approximately 670 Å, 730 Å, and 860 Å, respectively. Samples No. 2 and No. 5 exhibited larger values compared to the others. Notably, the smallest crystallite size for Ni_3Al was observed in sample No. 3 (≅ 360 Å). Both solid and liquid-phase sintering processes increased the Al lattice parameter, indicative of the formation of an Al-based solid solution. $NiAl_3$ was characterized by an orthorhombic lattice within the *Pnma* space group defined by the three lattice parameters *a*, *b*, and *c*.

The microstructure of sample No. 1, prepared from the elemental powder mixture through solid-phase sintering and subsequent hot deformation *via* forging at 530–540°C, is presented in Fig. 3. Significant porosity is evident in the synthesised material (Fig. 3, *a*). Silicon inclusions are uniformly distributed throughout the structure, with an average particle size of 50–70 μm. In addition, the structure contains

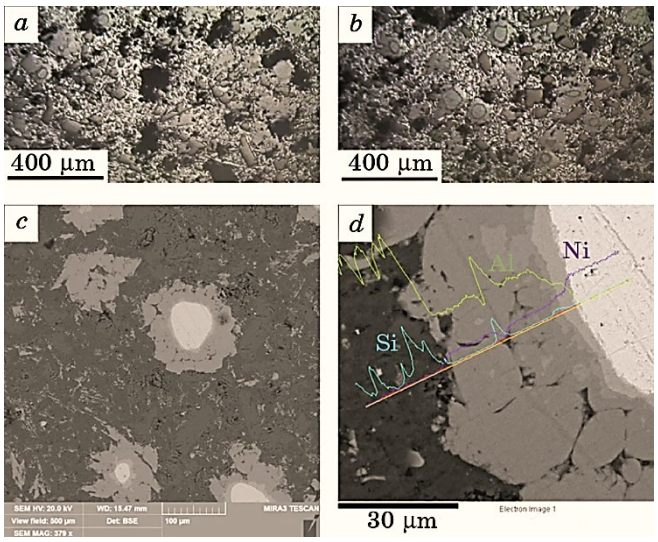

Fig. 3. Microstructure of material produced from a pure components mixture after solid-phase sintering and hot forging at 530–540°C (sample No. 1).

components in the form of rounded inclusions with a surrounding rim (Fig. 3, *b*). Based on the XRD analysis of this sample, these inclusions are likely nickel particles encased in a layer of Al_3Ni intermetallic.

To confirm the origin of these particles, an electron microscopy study coupled with energy-dispersive x-ray spectroscopy (EDS) analysis was conducted (Fig. 3, *d*). The grey background consists of a mixture of Al and Si phases, while the Ni core components attached to intermetallics were examined in details. Most of the intermetallic shell consists of $NiAl_3$, as previously observed in the XRD patterns. The aggregates identified in the structure (see Fig. 3, *c*) correspond to nickel particles surrounded by intermetallics, suggesting that the structure is not in equilibrium.

The hot forging process in this instance does not disrupt such aggregates. A thin (2–3 μm) layer of another intermetallic with a higher Ni content may also be present.

The most favourable structural characteristics were obtained for sample No. 2, produced from ball-milled master alloy powder after solid-phase sintering and hot forging at 520°C. Before forging, the sintered samples underwent preliminary hot pressing from the sides, achieving a set deformation degree of approximately 20–30% at 510–520°C. The microstructure of the material produced in this manner is shown in Fig. 4.

Silicon particles are evenly distributed within the metal matrix and are relatively small, with sizes ranging from 1 to 7 μm, significantly

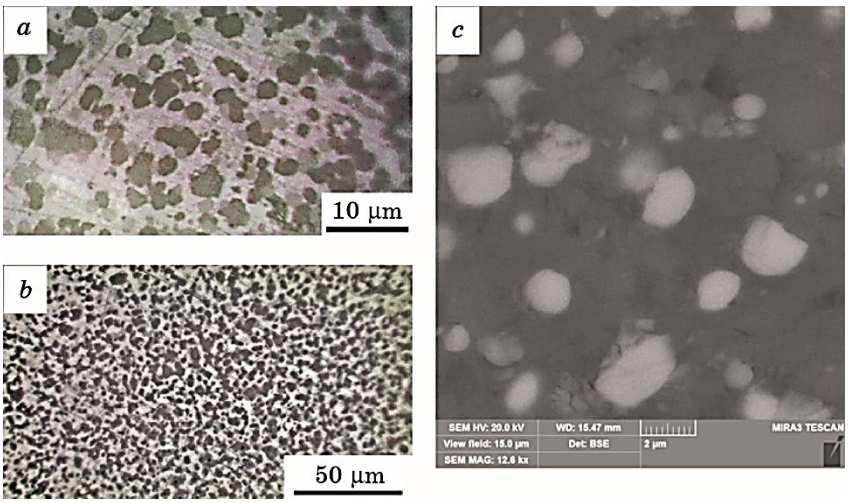

Fig. 4. Microstructure of material from pre-alloyed/master powder after solid-phase sintering and hot forging at 520°C (sample No. 2).

smaller than those in the other cases studied do. Based on the obtained structural indicators, this manufacturing method appears more suitable for further production. An SEM image of the structure of sample No. 2, which exhibited the best characteristics, is presented in Fig. 4. The intermetallic inclusions are spherical, with sizes of approximately 1–3 μm.

The microstructures of specimens produced from pre-alloyed powder after liquid-phase sintering and hot forging at 520–540°C are depicted in Fig. 5. Cast-like structures are visible in some areas (Fig. 5, *a*, *c*), with defects (pores) observed in these regions. The majority of the structure, however, consists of equiaxed polyhedral silicon particles. These inclusions exhibit a wide size range, from ≅ 5 μm to ≅ 60 μm, with an average size of 26.4 ± 4.7 μm.

Reducing the forging temperature to 520°C and incorporating side hot pre-pressing resulted in some improvement in the structure (Fig. 5, *b*, *d*). Despite this, the silicon inclusions were larger than those observed after solid-phase sintering were. The inclusions were homogeneously distributed, and cast-like structures as well as significant pores were not present. The inclusion sizes varied from ≅ 5 μm to ≅ 40 μm, with an average size of 19.8 ± 2.3 μm.

Although it is possible to mitigate porosity and cast structures after liquid-phase sintering, the large initial cast silicon crystals result in larger inclusions following deformation. Additionally, liquid-phase exudation can uncontrollably distort the chemical composition. Spectral analysis of the samples after liquid-phase sintering revealed an increase in Si content to approximately 40%.

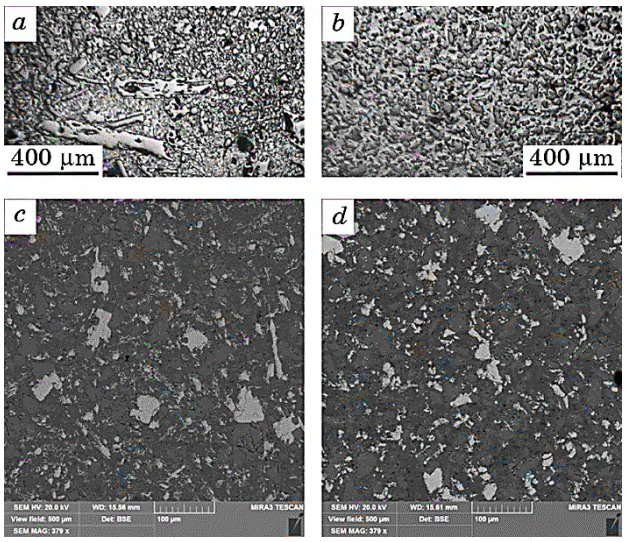

Fig. 5. Microstructure of material from pre-alloyed powder after liquid-phase sintering and hot deformation: forging at 530–540°C, regions with cast-like structures and pores (sample No. 3) (*a*, *c*), forging at 520°C with side pressing at 510–520°C (sample No. 4) (*b*, *d*).

Figure 6 illustrates the microstructure of sample No. 5, fabricated from a powder mixture after liquid-phase sintering and hot deformation. In this instance, slightly less porosity was observed compared to the undeformed state. The specific intermetallic inclusion structures identified after solid-phase sintering were not observed here.

The microstructure (Fig. 6, *a*) consists mainly of elongated Si particles embedded in the Al matrix. These silicon inclusions have a broad size range, from $\cong 10$ μm to $\cong 100$ μm, with an average size of 35.6 ± 6.3 μm. The elongated shapes are likely a result of deformation during the forging process, which aligns the inclusions along the direction of applied force.

Interestingly, the XRD analysis of sample No. 5, produced from the powder mixture through liquid-phase sintering and subsequent hot deformation, revealed no significant difference in phase composition compared to sample No. 1, which underwent solid-phase sintering. However, the microstructural examination highlighted notable disparities in the distribution and morphology of phases. The microstructure of sample No. 5 displayed a coarser and more heterogeneous distribution of Si particles compared to sample No. 1. This discrepancy is attributed to the presence of liquid phases during sintering, which facilitated the growth and coalescence of Si particles.

The microstructural analysis clearly shows that the method of sintering and the nature of the initial powder significantly influence the

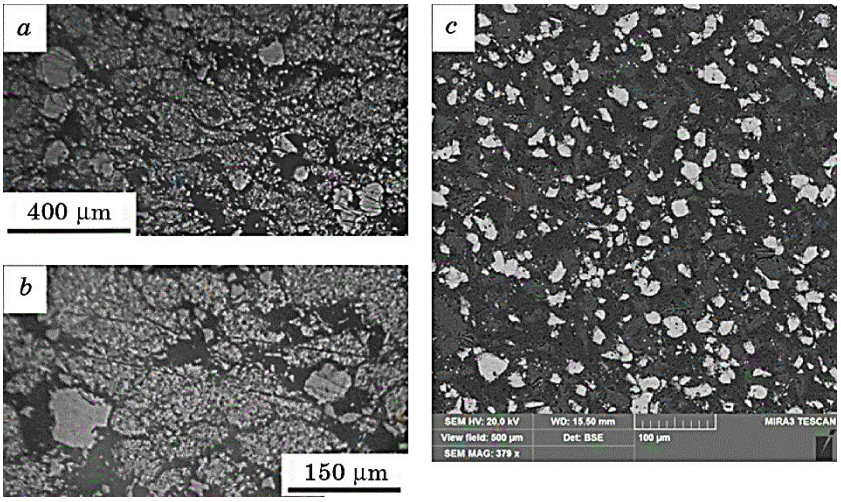

Fig. 6. Microstructure of material from elemental components mixture after liquid-phase sintering and hot deformation at 540–550°C (sample No. 5).

final properties of the material. Solid-phase sintering, especially when combined with hot forging, appears to produce a more uniform microstructure with finer Si particles, which is preferable for enhancing mechanical properties.

The mechanical properties of the sintered and forged samples were evaluated through hardness testing and tensile strength measurements. The results are summarised in Table 4.

Sample No. 2, produced from master alloy powder *via* solid-phase sintering and hot forging, exhibited the highest hardness and tensile strength. These superior properties can be attributed to the fine and homogeneous microstructure obtained through this manufacturing process. In addition, this material exhibited some ductility; however, not significant: values of total elongation reduction of the area were not more than $\cong 2\%$. Nevertheless, the other types of samples appear brittle without any noticeable signs of plasticity at home temperature.

All the other studied types of samples have significantly lower

TABLE 4. Effect of sintering conditions on the mechanical properties.

Sample number	σ_Y, MPa	σ_U, MPa	Hardness, *HB*
1	–	81.3 ± 27.2	68.1 ± 5.3
2	220.7 ± 10.3	261.2 ± 20.9	95.8 ± 3.2
3	–	116.6 ± 10.5	76.9 ± 4.5
4	–	139.7 ± 12.4	82.5 ± 5.7

TABLE 5. CTE values of the material at the studied temperatures.

Samples type	CTE at the temperature, $K^{-1} \cdot 10^6$					
	50°C	100°C	150°C	200°C	250°C	300°C
As-cast alloy		13.2		14.2		
Solid state sintering and forging (No. 2)	13.81	14.98	15.42	15.84	16.19	16.52
Liquid phase sintering and forging (No. 4)	10.51	12.95	13.18	13.49	13.82	14.13

strength and hardness values, which are caused by larger and rough-shaped silicon inclusion in addition to porosity. Among them, the strongest were the samples made of the pre-alloyed powder after liquid phase sintering and deformation regime close to the solid phase sintered previously considered one, which was almost nonporous. The highest ultimate tensile strength shown for such material was 145.4 MPa. Samples made of pure components mixture exhibit the lowest strength and are very brittle.

As it was mentioned in the introduction, except for obtaining appropriate mechanical properties this material needs to have a relatively low CTE close to those of steel. To check its value dynamometric tests were carried out. The results of these tests are given in Table 5. Because of liquid phase exudation liquid, which leads to significant silicon content increase, the corresponding samples exhibit lower CTE values. Pores also contribute to its decline. In the samples that had solid-state sintering and hot forging, which shoved the best mechanic properties, its value at lover temperatures is $13.81 \cdot 10^{-6}\ K^{-1}$. It is quite close to CTE of steel, which could be about $\cong (11-15) \cdot 10^{-6}\ K^{-1}$. However, for plain low-alloyed and carbon steels, it is about $\cong (11-12) \cdot 10^{-6}\ K^{-1}$, which is a bit less than the studied here material. The closest CTE matching shows Cr and Ni alloyed stainless steels, high Cr instrumental steels, and special Cr and Co alloyed steels.

Annealing after deformation does not make a valuable impact on the CTE of the material. However, it could be assumed that some rise of it might be observed, especially for the higher temperatures.

4. CONCLUSIONS

An experimental investigation was carried out to develop an optimised manufacturing process for a high-silicon Al–Si–Ni alloy with a coefficient of thermal expansion comparable to that of steels, using powder metallurgy techniques. In addition to the conventional pressing and sintering stages, hot forging was introduced to mitigate porosity and refine the morphology of silicon inclusions, thereby enhancing the ma-

terial properties. Both liquid and solid-phase sintering regimes were examined for materials produced from elemental powder mixtures and ball-milled pre-alloyed powders.

The results demonstrated that the optimal microstructure and properties were achieved using the following method: production of alloy powder through mechanical grinding of a rapidly solidified strip, compaction of the powder into a low-carbon steel shell at a pressure of 500–600 MPa, vacuum sintering (30 minutes at 350°C followed by 2 hours at 530°C), hot side setting with 20–30% deformation at 510–520°C, and hot forging at 520°C. This process resulted in a non-porous material with homogeneously distributed, fine, spherical silicon inclusions ranging in size from 1 to 7 μm.

Liquid-phase sintering was deemed impractical for the production of this material due to the exudation of the liquid phase, which uncontrollably alters the chemical composition of the material and promotes the formation of pores and voids. Furthermore, even if mechanical means were employed to prevent exudation, the presence of silicon crystals in the liquid phase would lead to their growth, resulting in coarse, cast-like structures with significantly reduced strength.

The use of elemental powder mixtures as a raw material was found to be highly undesirable. Instead, a pre-alloyed powder with the specified composition is recommended, which can be obtained by methods such as grinding a rapidly solidified strip. During solid-state sintering of elemental powder mixtures, nickel, which is insoluble in solid aluminium, tends to form coarse intermetallic aggregates that may include non-equilibrium compounds. Materials produced in this manner also exhibited porosity even after hot forging.

The study further revealed that the manufacturing method significantly influences the crystallite sizes for the Al and Si phases. These regions were found to be approximately 1.5 to 2.0 times larger after solid-phase sintering compared to liquid-phase sintering, regardless of whether the samples were manufactured from powder mixtures or pre-alloyed powders. In liquid-phase sintering, samples with larger coherent scattering regions may exhibit a finer overall structure. Additionally, a minor effect on the lattice parameters of the Al phase and $NiAl_3$ was observed.

As a result, the material developed in this study exhibits high mechanical properties (yield strength $\sigma_Y \cong 221$ MPa, ultimate tensile strength $\sigma_U \cong 261$ MPa, and hardness $\cong 96$ HB), with a coefficient of thermal expansion that meets production requirements, demonstrating its suitability for industrial application.

REFERENCES

1. V. I. Razumovskii and Y. K. Vekilov, *Phys. Solid State*, **53**: 2189 (2011).
2. R. Eliot, *Eutectic Solidification Processing. Crystalline and Glassy Alloys*

(Elsevier: 1983).
3. S. G. Alieva, M. B. Altman, and S. M. Ambartsumyan, *Promyshlennye Alyuminievyye Splavy* [Industrial Aluminium Alloys] (Moskva: Metallurgiya: 1984) (in Russian)
4. V. Vasenev, V. Mironenko, V. Butrim, A. Aronin, and I. Aristova, *Int. Conf. 'Powder Metallurgy and Particulate Materials'* (2013), p. 606.
5. E. L. Rooy, *Properties and Selection: Nonferrous Alloys and Special-Purpose Material* (ASM International: 1990), vol. **2**, p. 3.
6. I. Arribas, J. M. Martin, and F. Castro, *Mater. Sci. Eng. A*, **527**, Iss. 16–17: 3949 (2010).
7. M. L. Delgado, E. M. Ruiz-Navas, E. Gordo, and J. M. Torralba, *J. Mater. Processing Technol.*, **162–163**: 280 (2005).
8. Su Shei Sia, *Development of Hypereutectic Al–Si Based P/M Alloys* (Birmingham: 2012).
9. E. Crossin, J. Y. Yao, and G. B. Schaffer, *Powder Metallurgy*, **50**, Iss. 4: 354 (2007).
10. E. L. Ortiz, W. R. Osyrio, A. D. Bortolozo, G. S. Padilha, J. Y. Yao, and G. B. Schaffer, *Metals*, **12**, Iss. 6: 962 (2022).
11. V. V. Kaverinsky, Z. P. Sukhenko, G. A. Baglyuk, and D. G. Verbylo, *Metallofiz. Noveishie Tekhnol.*, **44**, No. 6: 769 (2022).
12. G. A. Bagliuk, T. O. Monastyrska, V. V. Kaverinsky, V. P. Bevz, V. K. Nosenko, I. M. Kirian, D. L. Pakula, V. V. Kyrylchuk, A. M. Lakhnik, and O. D. Rud, *Metallofiz. Noveishie Tekhnol.*, **45**, No. 8: 951 (2023).
13. L. Luterotti and S. Gialanella, *Acta Mater.*, **46**: 101 (1998).